# Development of the reference model for a residential heat pump system for cooling mode fault detection and diagnosis[†]

Minsung Kim[1,*], Seok Ho Yoon[2], W. Vance Payne[3] and Piotr A. Domanski[3]

[1]*New and Renewable Energy Department, Korea Institute of Energy Research, Daejeon 305-343, Korea*
[2]*Department of Energy Plant, Korea Institute of Machinery and Materials, Daejeon 305-343, Korea*
[3]*HVAC&R Equipment Performance Group, National Institute of Standards and Technology, Gaithersburg, MD 20899-8631, USA*

---

## Abstract

Development of a reference model to predict the value of system parameters during fault-free operation is a basic step for fault detection and diagnosis (FDD). In order to develop an accurate and effective reference model of a heat pump system, experimental data that cover a wide range of operating conditions are required. In this study, laboratory data were collected under various operating conditions and then filtered through a moving window steady-state detector. Over five thousand scans of steady-state data were used to develop polynomial regression models of seven system features. A reference model was also developed using an artificial neural network (ANN), and it is compared to the polynomial models.

*Keywords*: Air conditioner; Artificial neural network; Fault detection and diagnosis; Heat pump; Polynomial reference model

---

## 1. Introduction

A survey of over 55000 air conditioning units in the United States showed that more than 90 % were operating with one or more kinds of faults [1]. In another study, the average operating efficiency of the 1468 roof top units surveyed was 80 % of designed performance with 63 % of these units having performance degradation due to refrigerant leakage [2]. An effective fault detection and diagnostic (FDD) system would prevent these losses and reduce the energy usage of the air conditioning equipment.

FDD systems recognize a set of key system performance parameters and function by comparing predicted fault-free parameter values to the current values, and analyzing their residuals. Thus, a reference model is required to estimate the fault-free system parameters at any operating condition. Since a FDD system model requires precise estimation of system parameters, generalized conventional analytical modeling techniques were replaced with empirical correlations in several studies [3, 4]. Lee et al. (1996) used an artificial neural network to relate the dominant symptoms and faults of an air-handling unit [5]. To improve the modeling capability of a FDD system, Li and Braun (2003) implemented a polyno-

mial/generalized neural network regression in their reference model, and they produced improved interpolation and extrapolation results for a roof top unit [6]. Navarro-Esbri et al. (2007) developed a low-data-requirement model based on neural networks for a water-to-water vapor compression system focused on refrigerant leak detection [7]. In this study we collected extensive data for cooling mode operation of a residential air-source heat pump, and evaluated multivariable polynomial and artificial neural network reference models for their ability to predict system features selected for the FDD scheme.

## 2. Development of a fault-free steady-state reference model

### 2.1 Tested heat pump system

The studied system was a R410A, 8.8 kW (2.5 ton) split residential heat pump with a Seasonal Energy Efficiency Ratio (SEER) of 13 [8]. The unit consisted of an indoor fan-coil section, outdoor section with a scroll compressor, cooling mode and heating mode thermostatic expansion valves (TXV), and connecting tubing. Both the indoor and outdoor air-to-refrigerant heat exchangers were of the finned-tube type. The unit was installed in environmental chambers and charged with refrigerant according to the manufacturer's specifications. Fig. 1 shows a schematic of the experimental setup indicating the measurement locations of temperature, pressure, and mass

Table 1. Measurement uncertainties.

| Measurement | Range | Total uncertainty at the 95 % confidence level |
|---|---|---|
| Individual temperature | -18~93 °C | ±0.3 K |
| Temperature difference | 0~28 °C | ±0.3 K |
| Air nozzle pressure | 0~1245 Pa | ±1.0 Pa |
| Refrigerant mass flow rate | 0~544 kg/h | ±1.0 % |
| Dewpoint temperature | -18~38 °C | ±0.4 K |
| Dry-bulb temperature | -18~40 °C | ±0.4 K |
| Total cooling capacity | 3~11 kW | 4.0 % |
| COP | 2.5~6.0 | 5.5 % |

Table 2. System features used in fault detection.

| Independent Features | | Dependent Features | |
|---|---|---|---|
| Outdoor dry-bulb temperature | $T_{OD}$ | Evaporator exit refrigerant saturation temperature | $T_E$ |
| Indoor dry-bulb temperature | $T_{ID}$ | Evaporator exit refrigerant superheat | $T_{sh}$ |
| Indoor dew point temperature | $T_{IDP}$ | Condenser inlet refrigerant saturation temperature | $T_C$ |
| | | Compressor discharge refrigerant temperature | $T_D$ |
| | | Condenser exit liquid line subcooled temperature | $T_{sc}$ |
| | | Evaporator air temperature change | $\Delta T_{EA}$ |
| | | Condenser air temperature change | $\Delta T_{CA}$ |
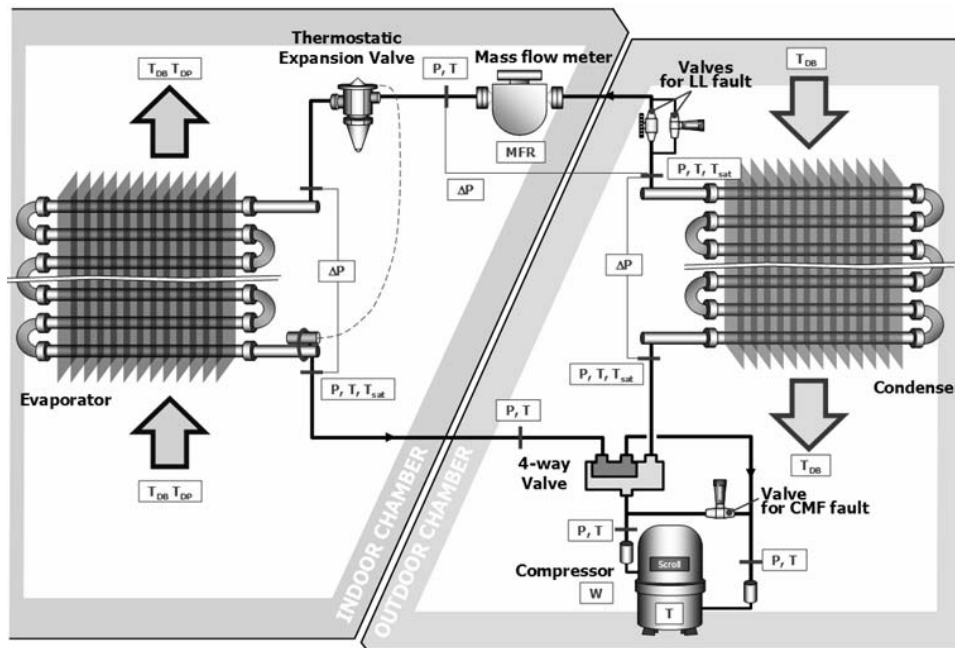


Fig. 1. Schematic diagram of the tested heat pump with measurement locations.

flow rate. On the refrigerant side, pressure transducers and T-type thermocouple probes were attached at the inlet and exit of every component of the system. The refrigerant mass flow rate was measured using a Coriolis flow meter. The air enthalpy method served as the primary measurement of the system capacity, and the refrigerant enthalpy method served as the secondary measurement. These two measurements always agreed within 5 %. Table 1 lists uncertainties of the major quantities measured during this work. Detailed specification of the test rig including indoor ductwork, dimensions, data acquisition, measurement uncertainty, and instrumentation was described in Kim et al. (2006) [9].

### 2.2 Steady-state detector

The large amount of test data needed to empirically model the cooling mode operation of a heat pump dictated that a consistent and automated method of data acquisition be implemented. For this purpose we used a steady-state detector which determined when the heat pump was in a steady state; thus, the steady-state detector qualified the data that were suitable for inclusion in the dataset used to generate the fault-free steady-state reference models.

The steady-state detector used in our data collection was described in detail by Kim et al. (2007) [10]. It focused upon the seven dependent features listed in Table 2. Fig. 2 shows a typical vapor compression cycle of a pure or pseudo-pure refrigerant like R410A. As seen in Fig. 2, the combination of seven dependant features of Table 2 explains the cycle in detail enough to describe current operating status. A moving window standard deviation technique was used for monitoring these variables and making a decision as to when steady state occurred. A moving window, as depicted in Fig. 3, was characterized by a time (or sample) interval over which each feature was sampled and saved. The average and standard deviation of the saved data within this time interval were calculated for each feature. The key to using the moving window tech-
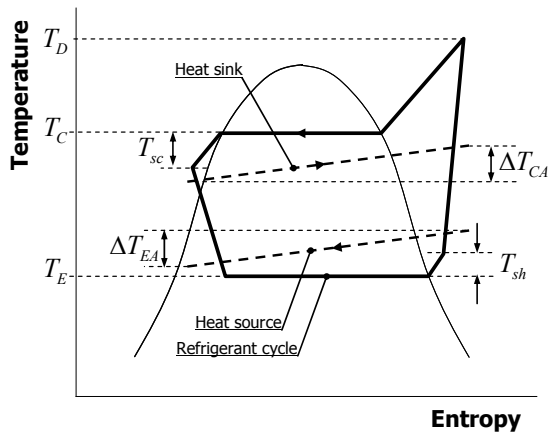
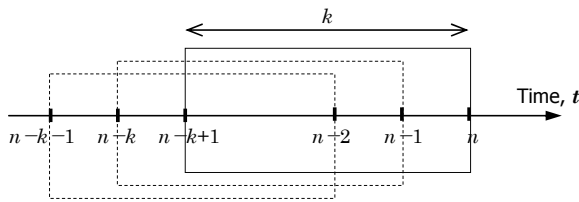Fig. 2. Temperature-entropy diagram of a typical vapor compression cycle.



Fig. 3. Moving window of k data points at $n^{th}$ time.

nique is determining the appropriate moving window size and the standard deviation threshold value for each feature below which the feature is defined to be at steady state.

To illustrate the technique, an example implementation of the steady-state decision is shown in Fig. 4(b) where the moving window standard deviation for $T_{sh}$ is shown. As $T_{ID}$ changes, features such as $T_{sh}$, $T_{sc}$, and $T_{EA}$ show instability. In this case $T_{sh}$ showed the most fluctuation and was the dominant feature in determining steady state (Fig. 4(c)).   In most cases, evaporator exit superheat and liquid line subcooling are the two features that determine the steady-state status, but they are not indicative of steady state for all operational conditions; therefore, the steady-state detector monitors all seven features, and all seven features' standard deviations within the moving window must be below their respective threshold values to indicate a steady system. A non steady-state condition for any one feature indicates that the system is not in steady state.

### 2.3 Experimental method and conditions

We systematically varied three independent variables, $T_{OD}$, $T_{ID}$, and $T_{IDP}$, and monitored the seven features. To implement the most efficient test procedure, outdoor temperature was fixed at one of four constant values, the addition of steam to the indoor chamber was set at one of several discrete levels by modulating a steam valve, and the indoor dry-bulb temperature was changed over the desired operating range by sequentially energizing ten fixed heaters. For example, as the number of indoor electric heaters increased, the test conditions moved from A to B in Fig. 5(a) with indoor temperature increasing.

Table 3. Operating conditions for fault-free tests.

| Independent Features | Conditions |
| --- | --- |
| Outdoor DB temp. (°C) | 27.8, 32.2, 35.0, 37.8 |
| Indoor DB temp. (°C) | 15.3 to 33.9 |
| Indoor humidity ratio | 0.0037 to 0.0168 |

The data were recorded continuously and filtered through the steady-state detector, which qualified steady-state data for use in development of the reference model. In this process, instability of the system due to on-off transients and rapid load changes was filtered out by the steady-state detector. The data in Fig. 5(b) were collected in a week.

Table 3 shows operating conditions for the fault-free tests. The four outdoor temperatures were maintained within ±0.3 °C. For the indoor conditions, the amount of steam introduced to the indoor chamber was fixed such that the humidity ratio varied from 0.0037 to 0.0168. Data were recorded, every 18 s, as indoor dry-bulb temperature varied from 15.3 °C to 33.9 °C. The range of operating conditions for which data were collected defines the applicable limits for the FDD scheme. The measurement interval was set in consideration of the specification of measuring equipment and data storage capacity. The measurement interval in this research was 13 s minimum due to a number of sensors as well as a large calculation capacity. Shorter interval will increase the model quality somehow; however, it may produce a large number of redundant data since the heat pump system is stabilized normally more than 10 minutes. In spite that a shorter measurement interval needs high cost for DAQ configuration, its contribution on the model quality is relatively small, also burdens computation capacity during model learning process.

From the total number of 10,409 recorded data sets, 5,830 data sets passed through the steady-state detector. Among these steady-state sets, 2,176 sets were collected at 27.8 °C outdoor temperature, 1,732 sets at 32.2 °C, 633 sets at 35.0 °C, and 1,289 sets at 37.8 °C. Fig. 5(b) shows a sample of data (every fifth data point) taken at four fixed outdoor temperatures. In addition, we performed ARI standard rating tests at 27.8 °C indoor and 35.0 °C outdoor dry-bulb temperatures [8] and included these data to develop the fault-free steady-state reference models.

### 2.4 Multivariable polynomial regression (MPR) reference model

The MPR model belongs to the "black-box" category of models, which do not consider the physics of the system and require a large data set to accurately predict a system's performance. In our study, we evaluated $1^{st}$, $2^{nd}$, $3^{rd}$, and $4^{th}$ order MPR models representing the seven key features of the heat pump. The higher order MPR models offer better accuracy of prediction; however, excessive polynomial order for a relatively small database may worsen data interpolation. The MPR models presented in this work have an advantage in that
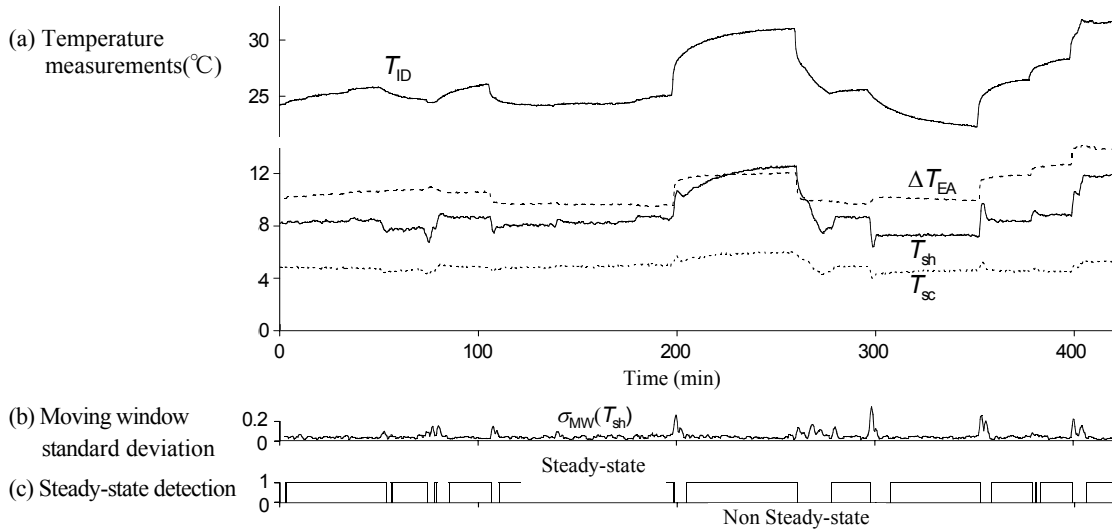
Fig. 4. Example of steady-state detection using the moving window standard deviations with $T_{sh}$ being the dominant feature; (a) Measurements of $T_{ID}$, $T_{EA}$, $T_{sh}$, and $T_{sc}$; (b) Moving window standard deviation of $T_{sh}$; (c) Steady-state status (yes=1, no=0).
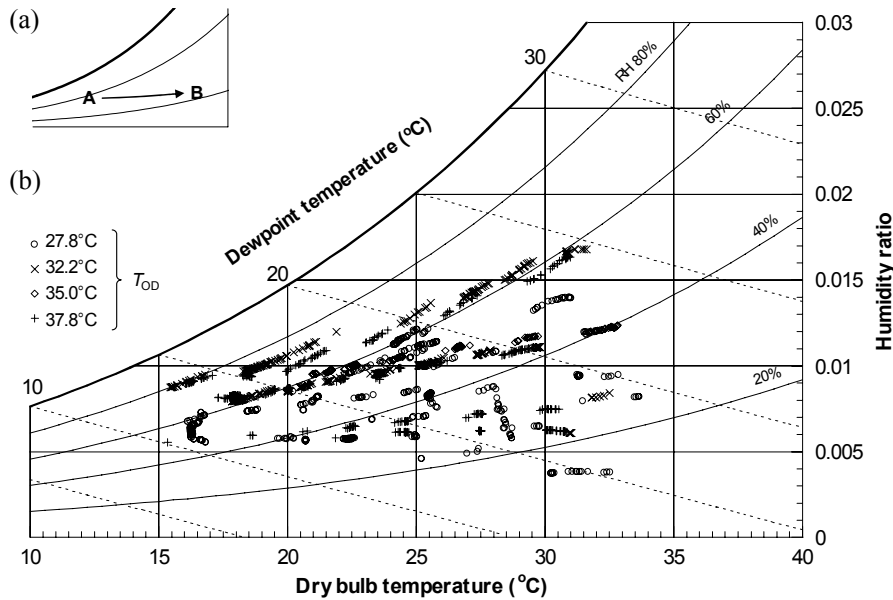


Fig. 5. Indoor test conditions on a psychrometric chart for fault-free model experiments at a fixed outdoor temperature; (a) Indoor condition change as electric heaters activate; (b) Sampled indoor air conditions at $T_{OD}$ of 27.8, 32.2, 35.0, and 37.8.

they have a simple structure and can be programmed easily. In addition, they can be implemented for any other experimental database with little modification, because they have no physical basis.

We used outdoor dry-bulb temperature ($T_{OD}$), indoor dry-bulb temperature ($T_{ID}$), and indoor dew point temperature ($T_{IDP}$) as independent variables. These variables were regressed upon the database generated from the fault-free tests. Eqs. (1a), (1b), (1c), and (1d) show the general form of the regressed equations for the $i$th feature (or $i$th dependent variable) as 1st, 2nd, 3rd, and 4th order MPR models, respectively.

$$\phi_i^{(1)} = a_0 + a_1 T_{OD} + a_2 T_{ID} + a_3 T_{IDP} \tag{1a}$$

$$\phi_i^{(2)} = \phi_i^{(1)} + a_4 T_{OD}^2 + a_5 T_{ID}^2 + a_6 T_{IDP}^2 + a_7 T_{OD} T_{ID} \\ + a_8 T_{ID} T_{IDP} + a_9 T_{IDP} T_{OD} \tag{1b}$$

$$\phi_i^{(3)} = \phi_i^{(2)} + a_{10} T_{OD}^3 + a_{11} T_{ID}^3 + a_{12} T_{IDP}^3 + a_{13} T_{OD} T_{ID} T_{IDP} \\ + a_{14} T_{OD}^2 T_{ID} + a_{15} T_{OD}^2 T_{IDP} + a_{16} T_{ID}^2 T_{OD} + a_{17} T_{ID}^2 T_{IDP} \\ + a_{18} T_{IDP}^2 T_{OD} + a_{19} T_{IDP}^2 T_{ID} \tag{1c}$$

$$\phi_i^{(4)} = \phi_i^{(3)} + a_{20} T_{OD}^4 + a_{21} T_{ID}^4 + a_{22} T_{IDP}^4 + a_{23} T_{ID}^2 T_{OD}^2 \\ + a_{24} T_{ID}^2 T_{IDP}^2 + a_{25} T_{IDP}^2 T_{OD}^2 + a_{26} T_{ID} T_{OD}^3 + a_{27} T_{ID} T_{IDP}^3 \\ + a_{28} T_{IDP} T_{OD}^3 + a_{29} T_{ID}^3 T_{OD} + a_{30} T_{ID}^3 T_{IDP} + a_{31} T_{IDP}^3 T_{OD} \\ + a_{32} T_{ID}^3 T_{OD} T_{IDP} + a_{33} T_{ID} T_{OD}^2 T_{IDP} + a_{34} T_{ID} T_{OD} T_{IDP}^2 \tag{1d}$$

### 2.5 Artificial neural network (ANN) reference model

An Artificial Neural Network (ANN) model was developed for the seven features. The relationship of independent variables and features is learned by an artificial neural network using a back propagation algorithm [11, 12]. Fig. 6 shows the structure of the ANN used in this study. It has three input variables ($T_{OD}$, $T_{ID}$, and $T_{IDP}$) and one output. This neural network has three layers consisting of an input, hidden, and output layer with the input and hidden layers having three nodes. The sigmoid function is used as the activation function of the hidden layer. The weight coefficients and offsets are "learned" using a momentum back propagation algorithm through an iterative way. Initial iteration required more than 10,000 iterations and took approximately 10 s with a Pentium-IV PC. The iteration time of the 3$^{rd}$ order MPR model was similar. The next iteration updating every single new data thereafter was reduced greatly. Though the number of iteration seems large, it took much shorter than expected because the calculation was a simple repetition of successive substitutive procedure without computation of matrix or thermophysical property.

The input layer acts only as input nodes; no processing of $T_{OD}$, $T_{ID}$, or $T_{IDP}$ occurs within the input layer. The various arrows between the input layer and the hidden layer indicate weights, or multipliers, applied to each input variable before passing to the sigmoid function within each hidden layer node. Eq. (2a) and Eq. (2b) illustrate the output of a neuron, $f(s)$, and how the sigmoid function is applied within the layers.

$$f(s) = \frac{1}{2}[1 + \tanh(2s)] \tag{2a}$$

$$s = \sum_{k=1}^{3} x_k w_k + c \tag{2b}$$

The three-node hidden layer uses 9 adjustable weighting coefficients and 3 offset coefficients. The single output node has its own 3 adjustable weighting coefficients and a single offset to produce the final predicted value of the feature, $F_{pred}$. Each heat pump feature to be represented by the ANN is calculated in this manner using $T_{OD}$, $T_{ID}$, or $T_{IDP}$ as inputs. The predicted value is compared to the measured value to produce an error value (residual) for each feature. The back propagation algorithm is then used to adjust the weights and offsets to minimize the error, or "train" the ANN.

## 3. Model validation

In validating the model, we used a dataset of 111 points, a subset of the full 5,830 point dataset, to improve the performance of the ANN learning process. The 111 point dataset was created by selecting the datapoints that were spaced by a minimum predetermined distance in the independent variables space. First, $T_{ID}$, $T_{OD}$, and $T_{IDP}$ were mapped onto *xyz*-coordinates. Each (x, y, z) point was then compared to all of the other points to determine if any of the other points fell within the predetermined distance of the point. This is equiva-

Table 4. MSR of the models fit to a reduced dataset of 111 points for the seven selected features.

| Feature | 1$^{st}$ order | 2$^{nd}$ order | 3$^{rd}$ order | 4$^{th}$ order | ANN |
|---|---|---|---|---|---|
| $T_E$ (°C) | 1.298 | 0.095 | 0.052 | 0.016 | 0.122 |
| $T_{sh}$ (°C) | 0.980 | 0.442 | 0.222 | 0.140 | 0.263 |
| $T_C$ (°C) | 0.136 | 0.014 | 0.007 | 0.005 | 0.072 |
| $T_D$ (°C) | 2.215 | 0.373 | 0.246 | 0.110 | 1.341 |
| $T_{sc}$ (°C) | 0.198 | 0.139 | 0.081 | 0.036 | 0.395 |
| $\Delta T_{EA}$ (°C) | 1.431 | 0.087 | 0.030 | 0.012 | 0.159 |
| $\Delta T_{CA}$ (°C) | 0.106 | 0.019 | 0.012 | 0.009 | 0.024 |
| m+1 | 4 | 10 | 20 | 35 | 16 |

Table 5. MSR of the models fit to the full dataset of 5830 points for the seven selected features.

| Feature | 1$^{st}$ order | 2$^{nd}$ order | 3$^{rd}$ order | 4$^{th}$ order | ANN |
|---|---|---|---|---|---|
| $T_E$ (°C) | 0.979 | 0.072 | 0.051 | 0.015 | 0.129 |
| $T_{sh}$ (°C) | 1.055 | 0.397 | 0.176 | 0.121 | 0.273 |
| $T_C$ (°C) | 0.108 | 0.011 | 0.007 | 0.005 | 0.068 |
| $T_D$ (°C) | 2.078 | 0.342 | 0.213 | 0.088 | 1.403 |
| $T_{sc}$ (°C) | 0.202 | 0.135 | 0.066 | 0.028 | 0.480 |
| $\Delta T_{EA}$ (°C) | 1.103 | 0.066 | 0.027 | 0.011 | 0.159 |
| $\Delta T_{CA}$ (°C) | **0.085** | **0.018** | **0.014** | **0.012** | **0.030** |
| m+1 | **4** | **10** | **20** | **35** | **16** |

Table 6. MSR of the reduced dataset model applied to the full dataset of 5830 points for the seven selected features.

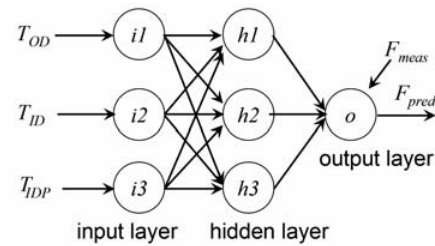| Feature | 1$^{st}$ order | 2$^{nd}$ order | 3$^{rd}$ order | 4$^{th}$ order | ANN |
|---|---|---|---|---|---|
| $T_E$ (°C) | 0.992 | 0.077 | 0.061 | 0.023 | 0.129 |
| $T_{sh}$ (°C) | 1.160 | 0.465 | 0.258 | 0.213 | 0.273 |
| $T_C$ (°C) | 0.110 | 0.012 | 0.0080 | 0.0078 | 0.068 |
| $T_D$ (°C) | 2.403 | 0.409 | 0.285 | 0.161 | 1.407 |
| $T_{sc}$ (°C) | 0.213 | 0.144 | 0.083 | 0.055 | 0.482 |
| $\Delta T_{EA}$ (°C) | 1.116 | 0.072 | 0.033 | 0.017 | 0.160 |
| $\Delta T_{CA}$ (°C) | 0.087 | 0.019 | 0.017 | 0.019 | 0.030 |
| m+1 | 4 | 10 | 20 | 35 | 16 |



Fig. 6. Artificial neural network structure.

lent to drawing a sphere of radius $r$ at a particular (x, y, z) location and examining this sphere volume to determine if any other points fall within. If another (x, y, z) point fell within this sphere, it was removed from the data set; thus all of the independent variable (x, y, z) points were examined and winnowed in this manner. In this study, $r$ was selected to be

0.96 °C.

Table 4 shows the mean squared residual (MSR), as calculated by Eq. (3), for the multivariate polynomial regression models and ANN model when fit to the reduced dataset consisting of 111 points. The mean squared residual is the sum of the squared residuals divided by the degrees of freedom for the regression and is an estimate of the model variance [13].

$$\text{MSR} = \frac{1}{N - (m+1)} \sum_i \left( x_i - \phi_i^{(n)} \right)^2 \tag{3}$$

Table 5 shows the MSRs for the models fit to the full dataset of 5,830 points while Table 6 shows the MSRs for the reduced dataset models applied to the full dataset. The reduced models' MSRs of Table 6 and the full dataset MSRs of Table 5 differ by an average of 26 %. Thus the reduced dataset is a good representation of the system features, but the full dataset model produces smaller MSRs.

As expected, a higher order MPR model produces a smaller mean squared residual. However, the number of model coefficients increases exponentially due to the addition of the cross-term coefficients. The number of coefficients, m+1, used to model each feature may be reduced by applying an F-Test to each coefficient of the respective models [13]. The F-statistic is calculated using the following equations:

$$\text{MS}_{\text{drop}} = \frac{1}{m-g} \left( \text{SSR}_{\text{reduced}} - \text{SSR}_{\text{full}} \right) \tag{4}$$

$$\text{MSR}_{\text{full}} = \frac{1}{N - (m+1)} \text{SSR}_{\text{full}} \tag{5}$$

$$F = \frac{\text{MS}_{\text{drop}}}{\text{MSR}_{\text{full}}} \tag{6}$$

where g+1 is the number of coefficients in the reduced model. The F-statistic follows an F distribution with m-g and N-(m+1) degrees of freedom. Large values of F indicate that the terms removed from the reduced model were significant. One may use the F-statistic as a means of ranking the contribution of a particular coefficient to the fit of the regressed model. By dropping one term at a time and sorting the reduced models in terms of their F-statistics, the effect of removal of a particular term may be assessed by comparing the MSR of the reduced model to that of the full model. Table 7 shows the results of this technique when applied to a backward elimination on the full 3$^{rd}$ order polynomial model.

Table 7 shows that one to four terms may be removed from the full 3$^{rd}$ order polynomial while the models' MSRs remain less than 1 % from the full models' MSRs. If the criteria is raised to within 5 % of the full models' MSRs, up to seven terms may be removed from several of the 3$^{rd}$ order polynomials. Raising the percentage change in MSR to within 10 % allows the removal of up to nine coefficients for $T_{\text{sh}}$. The decision as to how many terms to remove is at the discretion of the model developer, but as with any regression equation, the confidence interval on the mean value of any of the features determined at a particular

value of the independent parameters will be larger for larger MSRs. The confidence interval is a function of the MPR model standard residual (MSR$^{0.5}$), the Student's t-value for the particular confidence level, and degrees of freedom [14].

Fig. 7 shows the performance of the full MPR models and ANN model during operation at a $T_{\text{OD}}$ of 27.8±0.3 °C. If an air conditioning system is installed in the field, $T_{\text{ID}}$ may change continuously according to indoor cooling load or thermostat settings. The three features, $T_{\text{sh}}$, $T_{\text{sc}}$, and $T_{\text{D}}$, are shown in Fig. 7 because they varied the most as indoor temperature changed. In Fig. 7(a) where there is an abrupt change in $T_{\text{ID}}$, the steady state of the system is broken, as indicated by the steady-state detector in Fig. 7(e).

Fig. 7(b), 7(c), and 7(d) show $T_{\text{sh}}$, $T_{\text{sc}}$ and $T_{\text{D}}$ as predicted by the 1$^{st}$, 2$^{nd}$, and 3$^{rd}$ order MPR models and the ANN model. The 3$^{rd}$ order MPR model shows the best fit to the measured data during steady-state operation. As the order of the polynomial model decreases, the fit to the experimental data set degrades. Predictions by the ANN model are worse than those by the 3$^{rd}$ order MPR model. Since ANN approach has been known for its superiority to fit nonlinear functions, the $T_{\text{sh}}$ predicted by the ANN model is comparable to that of the 3$^{rd}$ order MPR model (Fig. 7(b)). However, $T_{\text{sc}}$ was not predicted well by the ANN model, as shown in Fig. 7(c). It means $T_{\text{sh}}$ has more non-linearity than other features where ANN approach shows superior matching. The predicted values of $T_{\text{D}}$ for the ANN model are between the 1$^{st}$ and 2$^{nd}$ order MPR models, as shown in Fig. 7(d).

## 4. Summary

Seven features of a residential heat pump system were modeled using the 1$^{st}$, 2$^{nd}$, 3$^{rd}$, and 4$^{th}$ order MPR models and an ANN model. The laboratory data were filtered by a steady-state detector, which automatically examined and processed data to improve data collection consistency and the resulting steady-state reference model. Considering the fit, the polynomial model should be at least 3$^{rd}$ order. The 4$^{th}$ order polynomial model's use of 75 % more coefficients for only a 14 % decrease in MSR does not justify it replacing the 3$^{rd}$ order model. The F-Test can be applied to reduce the number of coefficients in a general linear model, and this technique may aid a developer in creating a more compact representation of the system features. The ANN model predicted all features with less accuracy than the 3$^{rd}$ order MPR model. Because of insignificant non-linearity between the independent variables and the features in the cooling mode, the ANN model's ability to fit nonlinear behavior did not provide any advantage over the 3$^{rd}$ order MPR models.

The reference model should not be over-specified by increasing the order of the MPR model. The model variance should be lower than that of independent variable measurements. The smaller the models' variances, the smaller their contribution to the overall uncertainty of the predicted features. The model developer must decide on an acceptable level of model variance based upon his FDD requirements and his ability to measure the independent variables and features.

Table 7. Terms removed from the 3rd order MPR model using an F-Test.

| Feature | Term(s) removed[1] | | |
|---|---|---|---|
| | Less than 1 % higher MSR | Less than 5 % higher MSR | Less than 10 % higher MSR |
| $T_E$ (°C) | $z$, $xy$, $z^2$ | $z$, $xy$, $z^2$, $x^2$, $y$, $y^3$ | NA[2] |
| $T_{sh}$ (°C) | $y^2$, $z$, $z^2$, $y^2z$, $x$ | $y^2$, $z$, $z^2$, $y^2z$, $x$, $y$, $z^3$ | $y^2$, $z$, $z^2$, $y^2z$, $x$, $y$, $z^3$, $y^2x$, $y^3$ |
| $T_C$ (°C) | $y$ | $y$, $y^2z$, $y^3$ | $y$, $y^2z$, $y^3$, $yz$, $z^3$ |
| $T_D$ (°C) | $x$, $y^3$ | $x$, $y^3$, $yz$, $x^2y$, $z^2y$, $xyz$ | $x$, $y^3$, $yz$, $x^2y$, $z^2y$, $xyz$, $z^2$ |
| $T_{sc}$ (°C) | $y$, $z^2$, $z^2y$, $y^3$ | $y$, $z^2$, $z^2y$, $y^3$, $y^2x$, $yz$, $z^2x$ | NA |
| $\Delta T_{EA}$ (°C) | $y$ | NA | $y$, $z$ |
| $\Delta T_{CA}$ (°C) | $x^2z$, $y$, $z^3$ | $x^2z$, $y$, $z^3$, $y^3$, $z$, $x^2y$, $xz$ | NA |

[1] 3rd Order MPR Model Backward Elimination, $x = T_{OD}$, $y = T_{ID}$, $z = T_{IDP}$

[2] NA:   The % change in MSR does not fall between the upper and lower bounds with the removal of a single coefficient.
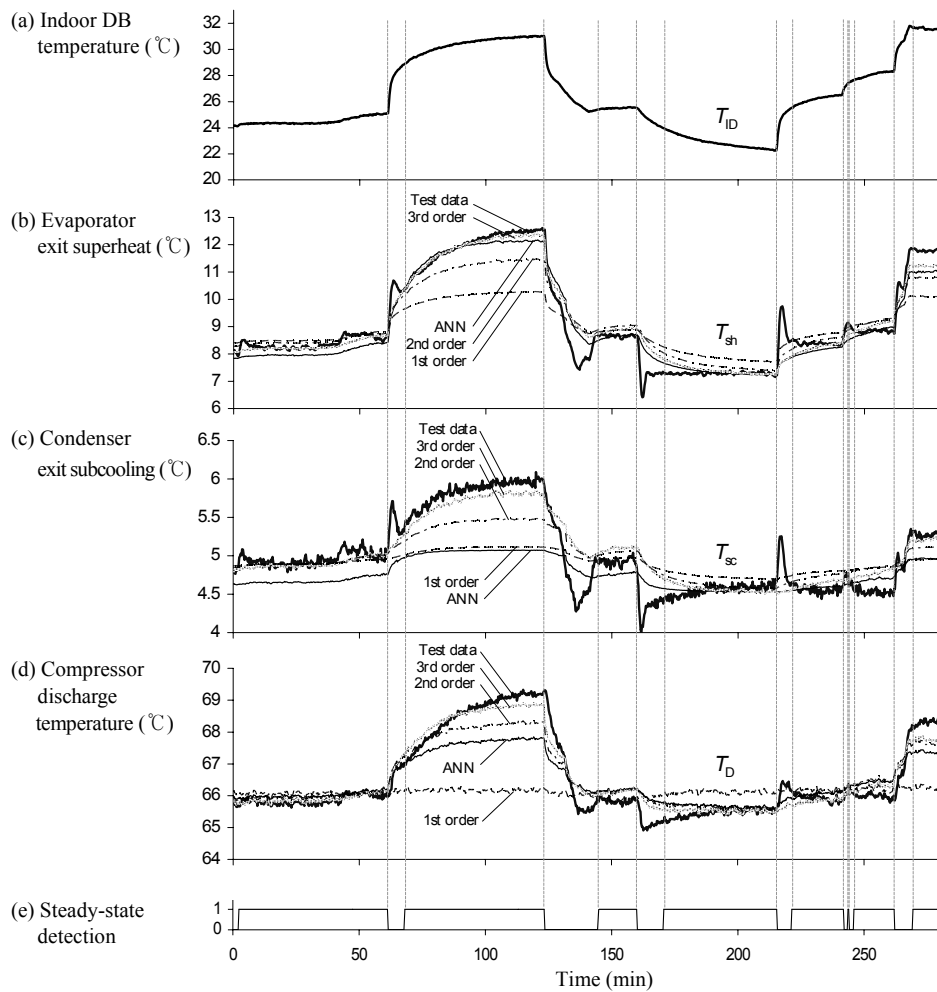


Fig. 7. Performance of MPR models and ANN model to predict features during a sample operation period; (a) $T_{ID}$; (b) $T_{sh}$; (c) $T_{sc}$; (d) $T_D$; (e) Steady-state status (yes =1, no = 0).

**Nomenclature**————————————————————

| | |
|---|---|
| $a$ | : Coefficient of multivariate polynomial |
| ANN | : Artificial neural network |
| $c$ | : Offset used in the sigmoid function |
| COP | : Coefficient of performance |
| CMF | : Compressor or reversing valve fault |

| | |
|---|---|
| DB | : Dry bulb |
| F | : Feature |
| FDD | : Fault detection and diagnosis |
| $g$ | : Number of coefficients minus one in a reduced model |
| $h1, h2, h3$ | : ANN hidden layer neurons |
| $i1, i2, i3$ | : ANN input layer neurons |
| LL | : Refrigerant liquid line |

m       : Number of coefficient in the regression model
MFR    : Mass flow rate
MPR    : Multivariate polynomial regression
MSR    : Mean squared residual
N        : Number of data samples used to generate the regression model
*o*       : ANN output layer neurons
*P*       : Pressure
*s*       : Variable used within the sigmoid function of Eq. (2)
SSR     : Sum of squared residuals
*T*       : Temperature (°C)
*w*      : Hidden node weighting factor for the $k^{th}$ input
*x*       : Input to hidden node of the ANN model

### *Greek symbols*

Δ       : Difference
$\phi^{(n)}$       : Feature or performance parameter of nth order model

### *Subscripts*

C        : Condenser
CA      : Condenser air
D        : Compressor discharge
drop    : Comparison of two identical models where one model has had some terms removed
E        : Evaporator
EA      : Evaporator air
full      : refers to the model with a complete number of coefficients
*i*        : Feature index
ID       : Indoor
IDP     : Indoor dew point
*k*       : Number of data samples in a moving window or input number in Eq. (2)
meas    : Measured
*n*       : Time index for moving window method
OD      : Outdoor
pred     : Predicted
reduced : refers to a model with some of the coefficients removed
sat       : Saturation
sc        : Subcooling
sh        : Superheat

### References

[1]  J. Proctor, Residential and Small Commercial Central Air Conditioning; Rated Efficiency isn't Automatic, in: Presentation at the Public Session. *ASHRAE Winter Meeting*, Jan. 26, Anaheim, CA, USA. (2004).

[2]  T. M. Rossi, Unitary Air Conditioner Field Performance, *International Refrigeration and Air Conditioning Conference at Purdue*, Paper No. R146, July 12-15, West Lafayette, IN, USA. (2004).

[3]  J. M. Gordon and K. C. Ng, Predictive and diagnostic aspects of a universal thermodynamic model for chillers, *Int. J. Heat Mass Trans.*, 38 (5) (1995) 807-818.

[4]  T. M. Rossi, Detection, diagnosis, and evaluation of faults in vapor compression cycle equipment, *Ph.D. Thesis, Purdue University*, West Lafayette, IN, USA. (1995).

[5]  W. -Y. Lee, J. M. House and G. E. Kelly, Fault Diagnosis of an Air-Handling Unit Using Artificial Neural Networks, *ASHRAE Transactions*, 102 (1) (1996) 540-549.

[6]  H. Li and J. E. Braun, An Improved Method for Fault Detection and Diagnosis Applied to Package Air Conditioners, *ASHRAE Transactions*, 109 (2) (2003) 683-692.

[7]  J. Navarro-Esbri, E. Torrella, and R. Cabello R., A vapour compression chiller fault detection technique based on adaptive algorithms. Application to on-line refrigerant leakage detection, *Int. J. Refrig.*, 29 (2007) 716-723.

[8]  ARI, *Performance rating of unitary air conditioning and air source heat pump equipment*, ARI Standard 210/240, Air Conditioning and Refrigeration Institute, Arlington, VA, USA. (2006).

[9]  M. Kim, W. V. Payne, P. A. Domanski and C. J. L. Hermes, *Performance of a residential heat pump operating in the cooling mode with single faults*, NISTIR 7350, National Institute of Standards and Technology, Gaithersburg, MD, USA. (2006).

[10]  M. Kim, W. V. Payne, P. A. Domanski and S. H. Yoon, Design of a steady-state detector for fault detection and diagnosis of a residential air conditioner, *Int. J. Refrig.*, 31 (5) (2008) 790-799.

[11]  P. D. Wasserman, *Neural Computing Theory and Practice*, *Van Nostrand Reinhold*, New York, NY, USA. (1989).

[12]  M. H. Hassoun, *Fundamentals of Artificial Neural Networks*, The MIT Press, Cambridge, MA, USA. (1995).

[13]  F. A. Graybill and H. K. Iyer, *Regression Analysis: Concepts and Applications*, 2nd ed., Duxbury Press, Belmont, CA, USA. (1994).

[14]  L. Ott, *An Introduction to Statistical Methods and Data Analysis 2nd ed.*, PWS Publishers, Duxbury Press, Boston, MA, USA. (1984).

**Minsung Kim** is a senior researcher of New and Renewable Energy Department at Korea Institute of Energy Research. He received Ph.D. degree in School of Mechanical and Aerospace Engineering from Seoul National University in 2002. His research interest includes residential and commercial heat pumps, building energy management, fault detection and diagnosis, and solar/geothermal energy applications. He recently worked on the development of industrial heat pump for high temperature generation.

**Seok Ho Yoon** is a senior researcher of Environment and Energy Systems Division at Korea Institute of Machinery and Materials. He received Ph.D. degree in School of Mechanical and Aerospace Engineering from Seoul National University in 2002. His research interest includes heat pumps, heat exchangers, and equipments of energy plant.



**W. Vance Payne** is a research engineer of HVAC&R Equipment Performance Group in National Institute of Standards and Technology (NIST). He received Ph.D. degree in Mechanical Engineering at Texas A&M University in 1997. His research has mainly focused on heat pumps and air conditioners, and recently on fault detection and diagnostics. He also worked on an alternate rating method for mixed system air-conditioners or heat pumps, on mass flow correlations for short tube expansion devices, and on HCFC replacement refrigerants.



**Piotr A. Domanski** is a leader of HVAC&R Equipment Performance Group in National Institute of Standards and Technology (NIST). He received Ph.D. degree in Mechanical Engineering at Catholic University of America in 1982. He dedicated himself in developing advanced heat pump simulation models like HPSIM, CYCLE-11, CYCLE_D, and EVAP-COND. Currently, Dr. Domanski's research focuses on the development of measurement science needed to improve the performance of HVAC equipment for building application in current and net-zero energy buildings. His interest covers evolutionary computation-based optimization methods, automated commissioning, and fault detection and diagnostics.